 CMC, vol.30, no.2, pp.177-194, 2012

Fracture Analysis of High strength and Ultra high strength Concrete beams by using Finite Element Method

A. Ramachandra Murthy[1], Nagesh R. Iyer[1] and B.K. Raghu Prasad[2]

Abstract: This paper presents the details of nonlinear finite element analysis (FEA) of three point bending specimens made up of high strength concrete (HSC, HSC1) and ultra high strength concrete (UHSC). Brief details about characterization and experimentation of HSC, HSC1 and UHSC have been provided. Cracking strength criterion has been used for simulation of crack propagation by conducting nonlinear FEA. The description about FEA using crack strength criterion has been outlined. Bi-linear tension softening relation has been used for modeling the cohesive stresses ahead of the crack tip. Numerical studies have been carried out on fracture analysis of three point bending specimens. It is observed from the studies that the computed values from FEA are in very good agreement with the corresponding experimental values. The computed values of stress vs crack width will be useful for evaluation of fracture energy, crack tip opening displacement and fracture toughness. Further, these values can also be used for crack growth study, remaining life assessment and residual strength evaluation of concrete structural components.

Keywords: High strength concrete; Ultra high strength concrete; Characterization; Finite element analysis

1 Introduction

Concrete has been one of the most commonly used construction materials in the world. One of the major problems civil engineers face today is concerned with preservation, maintenance and retrofitting of structures. The historical development of concrete material may be marked and divided into several stages. The first is the traditional normal strength concrete followed by high strength concrete, high performance concrete and reactive powder concrete/UHSC. Since UHSC is a rela-

[1] CSIR-Structural Engineering Research Centre, Taramani, Chennai, India, 600113, [murthyarc, nriyer] @serc.res.in

[2] Civil Engineering Dept., Indian Institute of Science, Bangalore, bkr@civil.iisc.ernet.in

tively new material, the fracture behaviour of this material is not well understood [Richard and Cheyrezy 1994, 1995, Mingzhe, et al. 2010, Goltermann, et al. 1997].

Concrete is a quasi-brittle material, which means its fracture process zone (FPZ) size is not small compared with the typical specimen or structural dimension. Classical linear elastic fracture mechanics (LEFM) approach is unable to predict the progressive failure of concrete specimens due to the presence of large FPZ of variable size ahead of the crack tip and the cohesive stress transferred within FPZ of the quasi-brittle materials like concrete (Bazant 2000). The LEFM based modeling approach assumes that once a crack propagates by a distance, this part of the material loses its load carrying capacity suddenly and completely. The complex nonlinear phenomena that take place in FPZ can be idealized and approximated using nonlinear fracture approaches to predict the localized physical behaviour in the vicinity of a crack and at the crack tip. Nonlinear fracture mechanics based approach recognizes that FPZ exists in front of the crack tip, in which the material can still carry loadings by mechanisms such as aggregate interlocking, surface friction and material bonding. As the crack propagates and opens, the material in FPZ softens with gradual energy dissipation, which can be accurately modeled by the fictitious crack model. The crack propagation direction is assumed to be perpendicular to the direction of the maximum stress at the cohesive crack tip. The cohesive crack model is one of such simplified nonlinear fracture models that can simulate satisfactorily the behaviour of concrete fracture. Inspired by the early stage of development of the fracture models (Barenblatt 1959, Dugdale 1960). Hillerborg, et al. (1976) initially applied cohesive crack method (or fictitious crack model) as a suitable nonlinear model for mode I fracture to simulate the softening damage of concrete structures. In the pioneering work, it was shown that analysis of crack formation and propagation as well as failure analysis could be conducted with cohesive crack model even if coarse finite element mesh was used thereby eliminating the mesh sensitivity. Ever since, a number of nonlinear fracture mechanics based models: crack band model (CBM) (Bazant and Oh 1983), two parameter fracture model (TPFM) (Jenq and Shah 1985), size effect model (SEM) (Bazant, et al. 1986), effective crack model (ECM) (Nallathambi and Karihaloo 1986), K_R-curve based on cohesive force (Xu and Reinhardt 1999a), double-K fracture model (DKFM) (Xu and Reinhardt 1999a, 1999b) and double-G fracture model (DGFM) (Xu and Zhang 2008) were proposed and used to predict fracture behaviour of concrete. Gomes and Awruch (2001) discussed the aspects related to three dimensional numerical modeling of RC structures using finite element method. The aspects include the solution technique for nonlinear equilibrium equations, constitutive model for concrete and steel. Zhang and Li (2004) simulated the crack propagation in fiber reinforced concrete by using fracture mechanics principles. Gasser and Holzapfel

(2005) carried out modeling of 3D crack propagation in unreinforced concrete using finite element method. Sancho, et al. (2007) presented a numerical technique for the modeling of cohesive crack based on the strong discontinuity approach. Stress vs crack opening law was used for modeling the crack. Ridha (2008) carried out nonlinear finite element analysis of high strength fiber reinforced concrete corbels. Compression behaviour of concrete was simulated by an elastic-plastic model and in tension fixed smeared crack model was used. Mehmet, et al. (2009) presented experimental and finite element analysis of steel fiber reinforced concrete beams subjected to four point bending. Dobromil (2010) improved the three dimensional fracture plastic model available in finite element software ATENA to capture fatigue damage in tension.

The nonlinear fracture models are based on two basic approaches: first by using finite element method (FEM) or boundary element method (BEM) and second by using modified LEFM concept. The cohesive crack model and crack band model fall under the former category, while two parameter fracture model, size effect model, effective crack model, K_R-curve based on cohesive force, double-K fracture model and double-G fracture model belong to latter group. The simplified assumptions and the ease with which FEM or BEM is applied in formulation of cohesive crack model are the main reasons of its popularity. In contrast to nonlinear models based on LEFM, cohesive crack model can satisfactorily capture the behaviour of an uncracked structure from crack initiation to the failure. The essential ingredient of the cohesive crack model is to use a proper shape of tension-softening relation (softening function) to characterize the fracture behaviour of cementitious materials. Figure. 1 represents the general characteristics of a softening function of concrete; in particular, it shows the variation of cohesive stress with respect to the crack opening displacement in FPZ. Material tensile strength f_t and the critical crack width w_c are the two important characteristic values of the softening function.

The main objective of this study is to conduct nonlinear finite element analysis of three point bending specimens made up of HSC, HSC1 and UHSC. To account for cohesive stresses, bi-linear tension softening model has been used.

2 Experimental Investigations

Three different mixes designated as HSC, HSC1 and UHSC are characterized and their mix proportions have been derived by using appropriate method and several trials. For HSC, the ingredient materials are Portland cement, coarse aggregate, fine aggregate and water, whereas for HSC1, the materials are Portland cement, silica fume, quartz sand, high range water reducer, water and steel fibers. Further, for UHSC, the materials are Portland cement, silica fume, quartz sand, quartz pow-

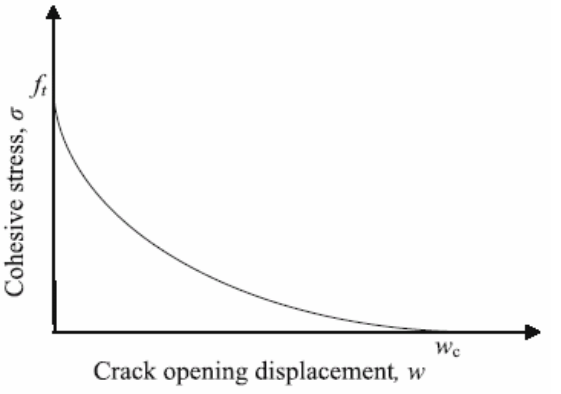

Figure 1: Representation of softening function of concrete

der, high range water reducer, water and steel fibers. The main difference between HSC1 and UHSC is the absence of quartz powder in the case of HSC1 mix. Bureau of Indian Standard code has been used for HSC mix design, whereas HSC1 and UHSC mixes have been designed based on the limited literature available and several trials. Several trials have been attempted before arriving at a final mix design. The final mix proportions and ratio obtained are given in Tables 1 and 2.

Table 1: Mix Proportions for HSC, HSC1 and UHSC

Property	HSC	HSC1	UHSC
Water/cement ratio	0.45	0.33	0.23
Cement, kg/m^3	452.44	811.7	838.93
Silica fume, kg/m^3	-	202.9	209.73
Quartz sand, kg/m^3	-	1217.5	922.82
Quartz powder, kg/m^3	-	-	335.57
Fine aggregate, kg/m^3	565.55	-	-
Coarse aggregate, kg/m^3	1127.01	-	-
Water, kg/m^3	203.6	267.9	192.95
Steel Fiber, kg/m^3		157.20	158.50
Superplasticizer(SP), (% weight of cement content in mix)	-	2.5%	3.5 %

Table 2: Mix of HSC, HSC1 and UHSC

Mix	Cement	Fine Aggregate	Coarse aggregate	Silica fume	Quartz sand	Quartz powder	Steel fiber	Water	SP %
HSC	1	1.25	2.48	-	-	-	-	0.45	-
HSC1	1	-	-	0.25	1.5	-	2%	0.33	2.5
UHSC	1	-	-	0.25	1.1	0.4	2%	0.23	3.5

2.1 Specimen Preparation

Preparation, demoulding and curing of HSC specimens is as usual, whereas the procedure for specimen preparation for HSC1 and UHSC is outlined below.

- A Hobart mixer machine (15 kg capacity) or Eirich type mixer (150 liter capacity) is used to mix the concrete mixtures.
- Well mixed dry binder powder is then slowly poured in to the bowl while the mixer is rotating at a slow speed.
- The speed of the mixer is increased and the mixing process is continued for about two to three minutes.
- Water is then added.
- Additional mixing is performed at this speed until a uniform mixture is achieved.
- Fibers are added after mixing all the ingredients such as cement, quartz sand, quartz powder and silica fume with water and superplasticizer.
- Fresh mixture is poured in to the moulds using a steel scoop.
- Compaction is done by placing the filled moulds on a laboratory table vibrator for about 2 minutes.
- The specimens are demoulded after a lapse of 24 hours.
- Immediately after demoulding, the specimens are fully immersed in potable water at room temperature for 2 days. After 2 days of normal water curing, the specimens are placed in a autoclave and maintained at 90˚C for 2 days. Further, the specimens are placed in oven and maintained at 200˚C for 1 day followed by autoclave curing.

2.2 Mechanical Properties

Various mechanical properties such as compressive strength, spilt tensile strength of HSC, HSC1 and UHSC mix at 28 days are shown in Table 3. From Table 3, it can be observed that the split tensile strength for the case of HSC is 4.0 MPa. It is about 7% of compressive strength. In the case of HSC1, the split tensile strength is about 18% of compressive strength. The increase in strength is large compared to HSC. The increase in strength may be due to various sizes of ingredients and steel fibres. Further, it can be observed from Table 3 that UHSC has high compressive strength and tensile strength. The high strengths can be attributed to the contribution at different scales viz., at the meso scale due to the fibers and at the micro scale due to the close packing of grains, which is on account of good grading of the particles.

Table 3: Mechnanical properties of HSC, HSC1 and UHSC

S. No	Mix ID	Compressive Strength (MPa)	Split tensile Strength (MPa)	Modulus of elasticity (MPa)
1.	HSC	57.14	3.96	35,780
2.	HSC1	87.71	15.38	37,890
3.	UHSC	122.52	20.65	42,987

2.3 Casting of Beams

Different beams, namely, small, medium and large size with various notch depths have been cast to study the fracture behaviour. The experimental setup consists of MTS 2500 kN capacity servo hydraulic UTM with online data acquisition system. All the specimens have been tested under displacement control at a rate of 0.02 mm/min. The mid-span downward displacement is measured using linear variable displacement transducer (LVDT), placed at center of the specimen under bottom of the beam. A clip gauge is used to measure the crack mouth opening displacement (CMOD). The data acquisition records load, CMOD, mid-span displacement and time. Appropriate load cells have been used for testing. A bi-linear tension softening model has been developed by using inverse analysis.

3 Simulation of Crack Propagation in Concrete Under Bending Load

There are two kinds of criteria that are generally used in the analysis of crack propagation in concrete. One is the strength criterion (Zhang and Stang 1998, Carpinteri, *et al.* 1998) and the other is the fracture toughness criterion (Li, et al. 1987, Zhang and Li 2004). Strength criterion is based on the assumption that the stress singularity at the crack tip is eliminated by the fictitious force in the FPZ around the

crack tip. Thus, the principal tensile stress at the crack tip (σ_{tip}) during the crack propagation should be equal to the cracking strength of concrete, i.e.

$$\sigma_{tip} = \sigma_{fc} \tag{1}$$

Fracture toughness criterion assumes that the stress singularity at the crack tip still exists and the fictitious force in the FPZ reduces the fracture toughness at crack tip, as in the double-K fracture model (Xu and Reinhardt 1999c, 2000). The total fracture toughness at crack tip (K_{tip}) is equal to the fracture toughness of cement matrix (K_{c-m}) and remains a constant during crack propagation, i.e.

$$K_{tip} = K_{c-m} \tag{2}$$

In the present study, cracking strength criterion has been used for obtaining the fracture parameters by conducting nonlinear finite element analysis. The details of simulation of crack propagation with strength criterion are discussed below.

3.1 Simulation of crack propagation with cracking strength criterion

Considering a central pre-notched concrete beam under three point bending load (refer Figure. 2), the direction of crack propagation should be perpendicular to the maximum principal stress. Therefore, the crack propagation path in this load condition can be predicted in advance, i.e. parallel to the load, from the notch tip upwards to the beam top. Here, the fictitious crack tip is defined as the point where the principal tensile stress attains the cracking strength σ_{fc} and the crack opening at this point is equal to zero. The material in FPZ is still able to transfer stress, which is governed by the crack opening displacement w. The relationship between the cohesive stress and the crack opening displacement can be expressed by a multi-linear equation, (Zhang, et al. 2010) i.e.

$$\sigma_n = k_n w + \sigma_{0n} \; for \; w_{n-1} \le w \le w_n \; (n = 1, 2, ..., n_{\max}) \tag{3}$$

where, k_n is the slope for $w \in [w_{n-1},\ w_n]$. $\sigma_{01} = \sigma_{fc}$,

$$\sigma_{0n} = \sum_{1}^{n-1} [(k_i - k_{i+1}) w_i] + \sigma_{fc}$$

Figure. 2 shows a cracked beam section with initial notch length a_0, crack length, a and external load P. The fictitious bridging stress acting on the crack surface along the cracking section is $\sigma_b(w(x))$. According to the principle of superposition shown in Figure. 2, the crack opening displacement along the crack length can be obtained by summing the contributions of external load and the bridging force, i.e.

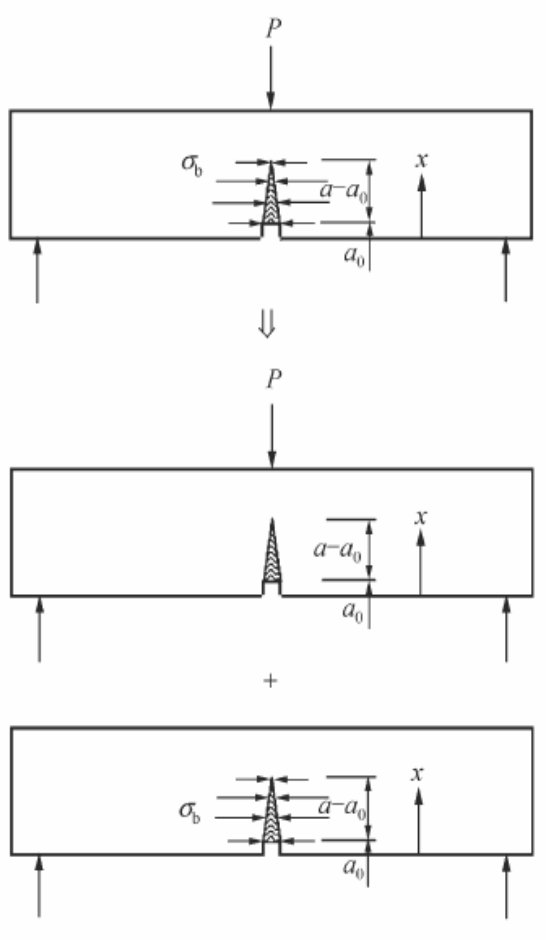

Figure 2: Principle of superposition in cracking concrete beam under bending load and fictitious force

$$w(x) = k_{pw}(x)P - t\int_0^a k_{fw}(x,y)\sigma_b(y)dy \quad for\ 0 \le x < a \tag{4}$$

Similarly, the stress a the crack tip can be obtained by

$$\sigma_{tip} = k_{p\sigma}P - t\int_0^a k_{f\sigma}(x,y)\ \sigma_b(y)\,dy\ for\ 0 \le x < a \tag{5}$$

As the equilibrium attained, $\sigma_{tip} = \sigma_{fc}$. k_{pw}, k_{fw} *and* $k_{p\sigma}$, $k_{f\sigma}$ are the influencing factors of external load and fictitious force on the crack opening and crack tip stress, respectively. Instead of solving the above equation by integration during iteration towards self-consistency to w(x), the problem can be solved in the matrix form, which can significantly enhance the computational procedures especially when many applied load levels need to be considered to improve the precision of the derived $\sigma - w$ relation. With reference to the bending specimen shown in Figure. 3, the nodes are distributed along the potential fracture line. The closing stresses acting on the crack surface are replaced by nodal forces that are governed by the crack opening displacement according to the $\sigma - w$ relationship of the material. When the cracking strength is attained at the crack tip, the node is then spilt into two nodes and a pair of opposite nodal forces starts to act on these two nodes. The fictitious crack tip then moves to next node.

Let vector $w \equiv (w_1, w_2, w_3, ...w_m)$, $F \equiv (F_1, F_2, F_3...F_m)$, and assume the node number of crack tip is m+1, then the equations 4 and 5 can be expressed in matrix form as:

$$w_i = k_{pw-i}P - \sum_{i=1}^{m} k_{fw-i}F_i \ (i = 1,2...,m) \tag{6}$$

$$\sigma_{fc} = k_{p\sigma}P - \sum_{i=1}^{m} k_{f\sigma-i}F_i \ (i = 1, 2...,m) \tag{7}$$

F_i can be related with w_i by

$$F_i = (k_n w_i + \sigma_{oi}) \ t \ \Delta l_i \ (i - 1,2,...,m) \tag{8}$$

where t is the specimen thickness and Δl_i is the length at node i. Here Δl is the distance between two adjacent nodes. Generally $\Delta l_i = \Delta l$ except for i = 1 when $\Delta l_i = 0.5\Delta l$. The influencing factors for the opening at each node and crack tip principal stresses are obtained by using finite element analysis, where the cracked beam shown in Figure. 3 is subjected to $m + 1 (P, F_1, .., F_m = 1)$ different loading condition. For a given fictitious crack length a (a=m Δl), equations 6, 7 and 8 turn into a linear algebraic system of (2m+1) equations and (2m+1) unknowns, i.e. $x \equiv (P, w_1, w_2, w_3, ...w_m, F_1, F_2, F_3, ...F_m)$. In addition, the crack mouth opening displacement w_0 can be related to P and F_i by

$$w_0 = k_{pw-0}P - \sum_{i=1}^{m} k_{fw-i}F_i \ (i = 1,2,...,m) \tag{9}$$

Thus, for a given crack length, a and stress–crack width relation, solving equations 6, 7 and 8, the critical external load capacity P, fictitious force F_i and crack profile w(x) can be obtained. The CMOD can then be calculated from equation 9. In the present investigation bi-linear tension softening model has been used to account for the cohesive stresses.

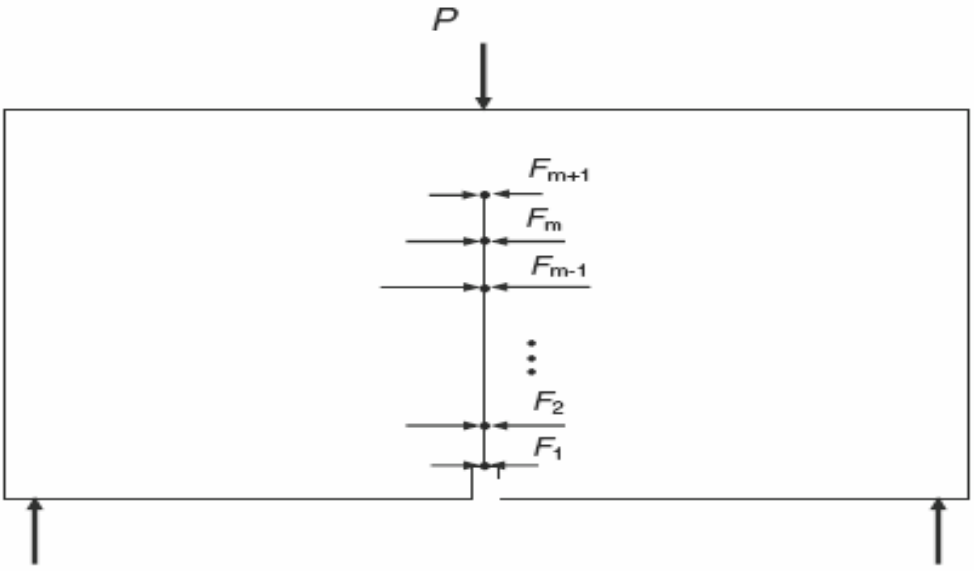

Figure 3: Finite element nodes and fictitious force on node along the Potential fracture line

4 Numerical Studies

Numerical studies have been carried out on fracture analysis of three point bending specimens made up of HSC, HSC1 and UHSC. Finite element analysis (FEA) has been carried out using the general purpose software, ABAQUS. Bi-linear tension softening relation has been used for modeling the cohesive stresses ahead of the crack tip. Details of fracture analysis of a HSC, HSC1and UHSC beams are given below.

4.1 FEA of HSC beam

Beam size = 1000*50*200mm, notch depth = 20mm

Modulus of elasticity = 35780 MPa, Maximum load = 7274 N (from experiments)

Tensile strength (f_t) = 3.75 MPa

Finite element modeling has been carried out by employing 8-noded solid element (C3D8). Aspect ratio of the element is kept less than 5.0. Figure. 4 shows FE mesh, loading and boundary conditions. Cracking load has been estimated by increasing the load in incremental manner by comparing the maximum principal stress with the material tensile strength. Figure. 5 shows the stress contour (σ_{11}) for the pre-notched beam including the zoomed view. Once, the maximum principal stress just exceeds the material tensile strength, the nodes have been released from the connecting elements at the crack tip. Then, equivalent force is applied to the nodes in the opposite direction of the crack opening. FEA has been carried out by increasing the external load on the beam till the maximum principal stress at the crack tip exceeds the tensile strength. This procedure is repeated till the crack width reaches critical crack width of the member, which is obtained from the experiments. Figure. 6 shows a typical stress contour (σ_{11}) for the cracked beam including the zoomed view.

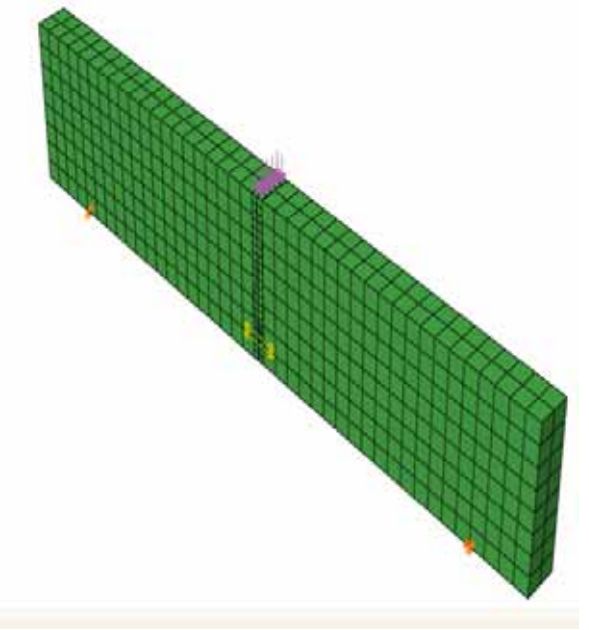

Figure 4: FE mesh, loading and boundary conditions

Figure. 7 shows the computed crack widths for various stress levels and comparison with experimentally obtained values. It is observed from Figure. 7 that the computed values from FEA are in very good agreement with the corresponding

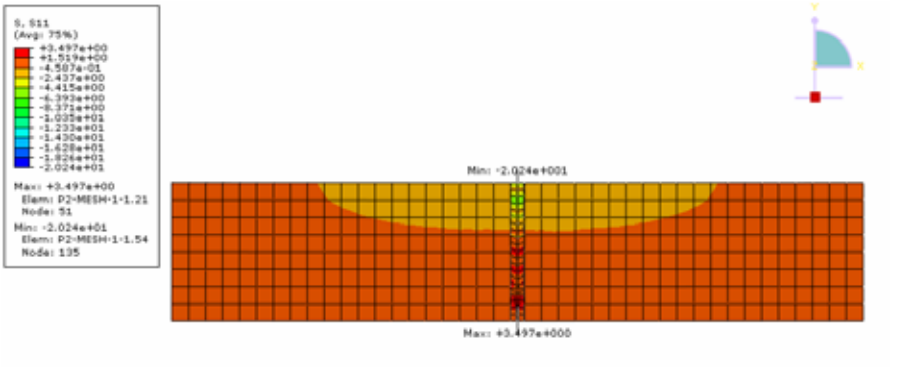

(a) Stress contour

(b) Zoomed view near crack tip

Figure 5: Stress (σ_{11}) contour with zoomed view

experimental values.

4.2 FEA of UHSC beam

Size of the beam = 650*50*130mm Notch depth = 13mm

Modulus of elasticity = 42987 MPa

FEA has been carried out for UHSC beam. Figure. 8 shows FE mesh, stress contours at various stages of crack propagation. Figure. 9 shows the response of FEA and comparison with the corresponding experimental values. It is observed from Figure. 9 that there is good agreement between FEA and the corresponding experimental values.

4.3 FEA of HSC1 beam

Similar procedure has been followed for the FEA of HSC1 beams. The details are given below.

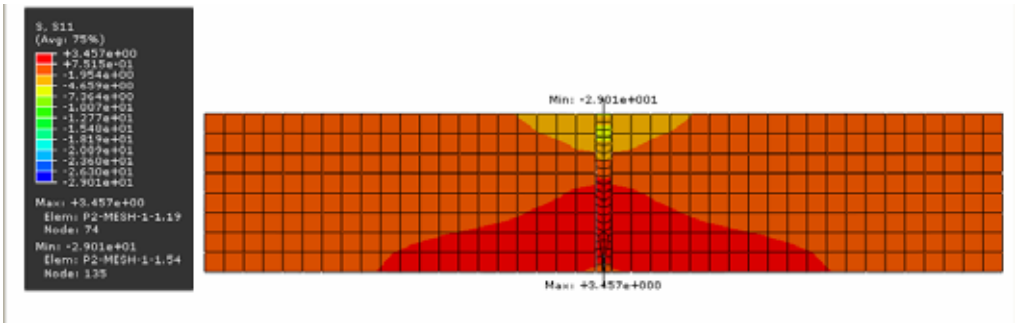

(a) Stress contour

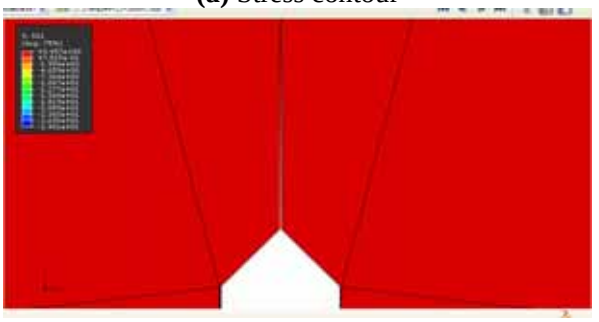

(b) Zoomed view near crack tip

Figure 6: Stress contour (σ_{11}) of the cracked beam with zoomed view

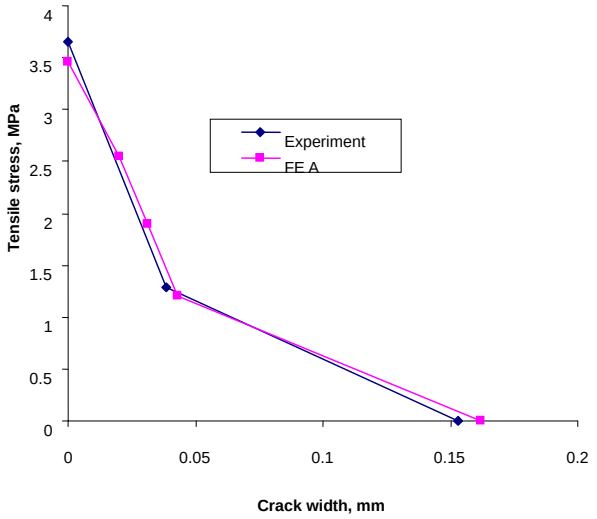

Figure 7: Tensile stress vs crack width-HSC

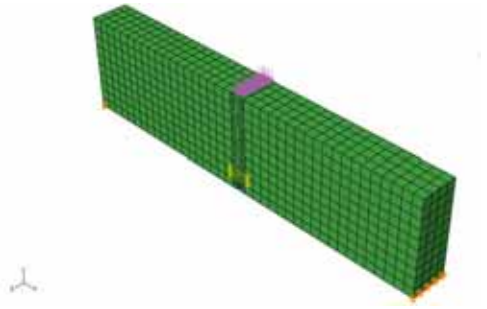

(a) FE mesh

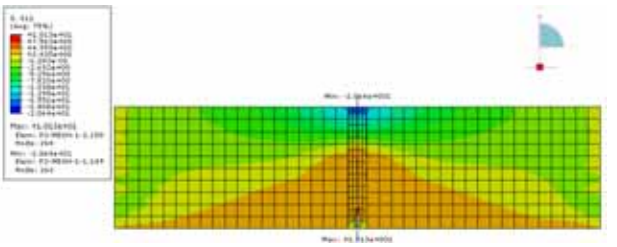

(b) Stress contour (σ_{11}) for the pre-notched beam

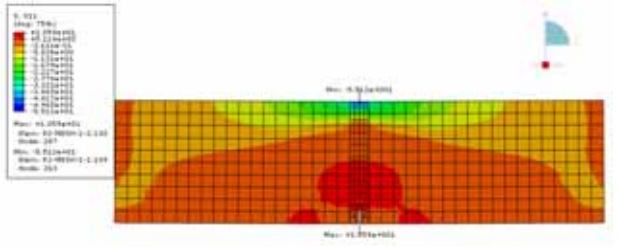

(c) Stress contour (σ_{11}) - I level
(elements failed in first row)

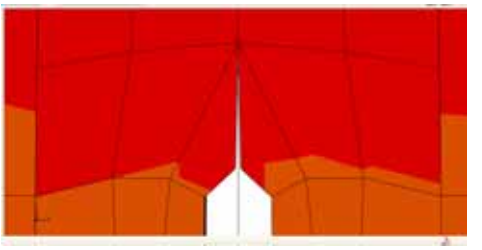

zoomed view near crack tip

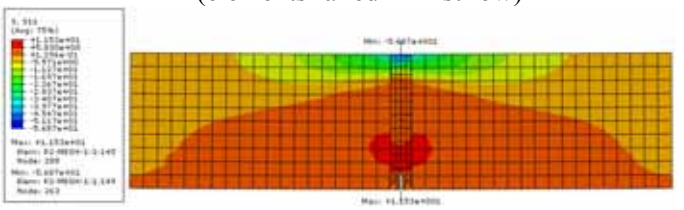

(d) Stress contour (σ_{11}) - II level
(two rows of elements failed)

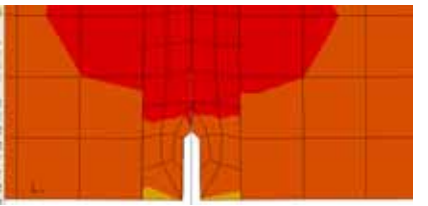

zoomed view near crack tip

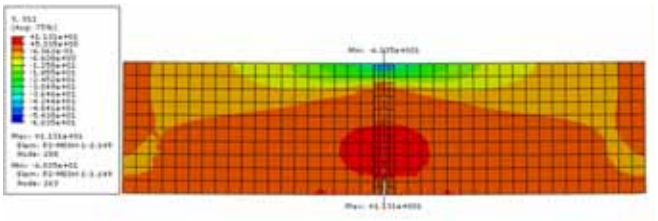

(e) Stress contour (σ_{11}) - III level
(three rows of elements failed)

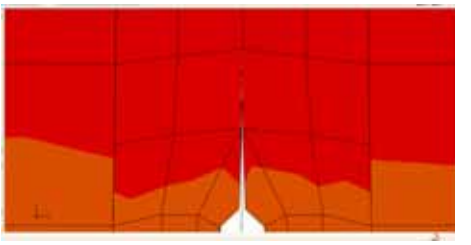

zoomed view near crack tip

Figure 8: FE mesh and stress contours with zoomed view

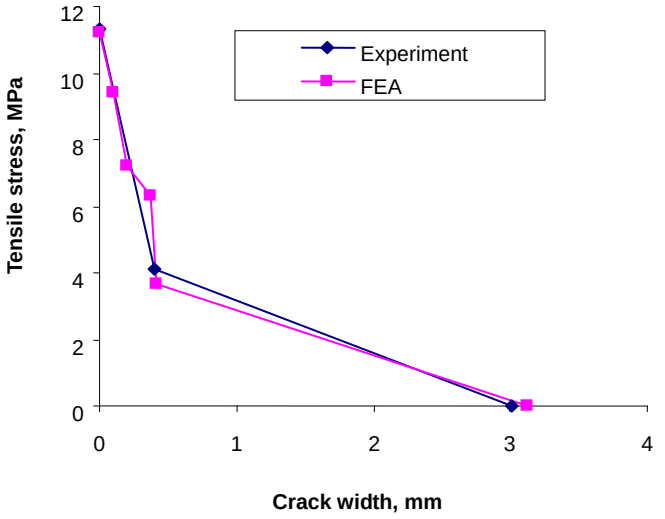

Figure 9: Stress vs crack width –UHSC

Size =500 X 50 X 100mm Notch depth =20mm Modulus of elasticity = 37,890 MPa

Figure. 10 shows the computed crack widths against tensile stress and the corresponding experimental values. From Figure. 10, it is observed that the computed values from FEA are in good agreement with those of the corresponding experimental values.

The computed values of stress vs crack width will be useful for evaluation of fracture energy, crack tip opening displacement and fracture toughness. Further, these values can also be used for crack growth study, remaining life prediction and residual strength evaluation.

5 Summary

Nonlinear FEA of three point bending specimens made up of HSC, HSC1 and UHSC has been carried out. Brief description about characterization and experimentation of HSC, HSC1 and UHSC has been outlined. Cracking strength criterion has been used for crack simulation by conducting nonlinear FEA. Strength criterion is based on the assumption that the stress singularity at the crack tip is eliminated by the fictitious force in FPZ around the crack tip. The details about FEA using crack strength criterion has been outlined. Bi-linear tension softening relation has been used for modeling the cohesive stresses ahead of the crack tip. Numerical

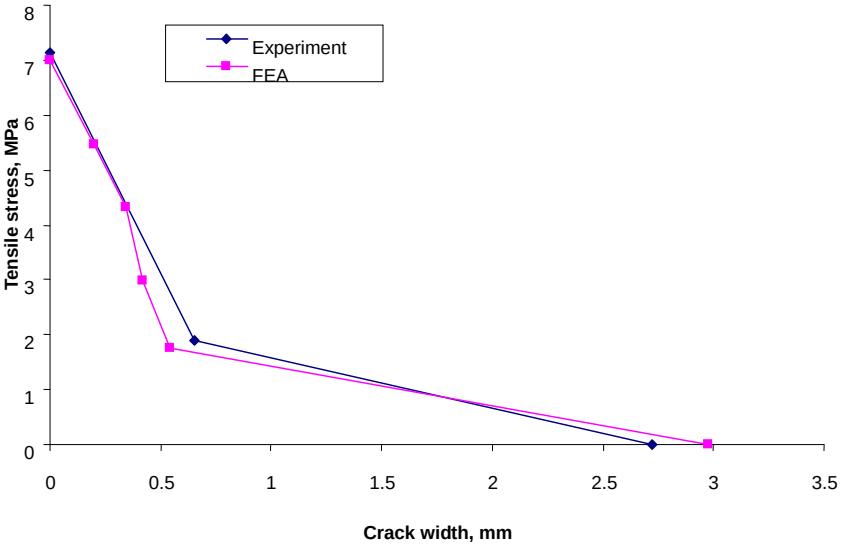

Figure 10: Stress vs crack width- HSC1 beam

studies have been carried out on fracture analysis of three point bending specimens. It is observed from the studies that the computed values from FEA are in very good agreement with the corresponding experimental values. The computed values of stress vs crack width will be useful for evaluation of fracture energy, crack tip opening displacement and fracture toughness. Further, these values can also be used for crack growth study, remaining life assessment and residual strength evaluation.

Acknowledgement: We acknowledge with thanks the valuable technical suggestions and support provided by our colleagues, Dr. G.S. Palani, Mr S. Maheshwaran, Ms. Smitha Gopinath, V. Ramesh Kumar, Scientists and B. Bhuvaneshwari, Quick Hire Fellow during the course of this investigation. The help and support provided by the staff of Advanced Materials Laboratory, CSIR-SERC to carry out the experiments is greatly acknowledged. This paper is being published with the permission of the Director, 2. CSIR-SERC, Chennai, India.

References

Barenblatt, G. I. (1959): The formation of equilibrium cracks during brittle fracture: general ideas and hypotheses, axially symmetric cracks. *Appl Math Mech,* 23, pp.622–36.

Bazant, Z. P. (2000): Size effect. *Int J Solid Struct*, 3, pp.69–80.

Bazant, Z. P.; Kim, J.K.; Pfeiffer, P. A. (1986): Determination of fracture properties from size effect tests. *J. Struc. Eng.,* ASCE, 112, pp.289–307.

Bazant, Z. P.; Oh, B. H. (1983): Crack band theory for fracture of concrete. *Mater. Struct.,* 16(93), pp.155–177.

Carpinteri, A.; Chiaia, B.; Ferro, G. (1998): Scale dependence of tensile strength of concrete specimens: a multifractal approach. *Mag. Concr. Res.*, 50, pp.237–246.

Dugdale, D. S. (1960): Yielding of steel sheets containing slits. *J Mech Phys Solids*, 8, pp.100–4.

Goltermann, P.; Johansen, V.; Palbol, L. (1997): Packing of Aggregates: An Alternate Tool to Determine the Optimal Aggregate Mix. *ACI Material Journal*, pp.435-443.

Gomes, H.M.; Awruch, A.M. (2001): Some aspects on three-dimensional numerical modelling of reinforced concrete structures using the finite element method. *Advances in Engineering Software*, 32, pp.257-277.

Hillerborg, A.; Modeer, M.; Petersson, P. E. (1976): Analysis of crack formation and crack growth in concrete by means of fracture mechanics and finite elements. *Cement Concrete Res*, 6, pp.773–82.

Jenq, Y. S.; Shah, S. P. (1985): Two parameter fracture model for concrete. *J. Eng. Mech., ASCE ,* 111(10), pp.1227–1241.

Li, V. C.; Chan, C. M.; Leung, C. K. Y. (1987): Experimental determination of the tension-softening relations for cementitious composites. *Cem. Concr. Res.*, 17,pp.441–452.

Maha Mohammed Saed Ridha (2008): Nonlinear finite element analysis of high strength fiber reinforced concrete corbels. *Engg. & Tech.*, 26, pp.1-15.

Mehmet Özcan, D.; Alemdar Bayraktar; Abdurrahman ?ahin; Tefaruk Haktanir; Temel Türker. (2009): Experimental and finite element analysis on the steel fiber-reinforced concrete (SFRC) beams ultimate behavior. *Construction and Building Materials*, 23, pp.1064-1077.

Mingzhe, A. N.; Ziruo, Y. U.; Sun Meili; Zheng Shuaiquan; Liang Lei. (2010): Fatigue Properties of RPC under Cyclic Loads of Single-stage and Multi-level Amplitude. *Journal of Wuhan University of Technology-Material Science Ed.,* pp.167-173.

Nallathambi, P.; Karihaloo, B. L. (1986): Determination of specimen-size independent fracture toughness of plain concrete. *Mag. Concrete Res.,* 38(135), pp.67–76.

Pryl Dobromil; Cervenka Jan; Pukl Radomir. (2010). Material model for finite element modelling of fatigue crack growth in concrete. *Procedia Engineering*, 2, pp.203-212.

Richard, P.; Cheyrezy, M. (1995): Composition of reactive powder concretes. *Cement & Concrete Research.,* 25(7), pp.1501-1511.

Richard, P.; Cheyrezy, M. H. (1994): Reactive powder concretes with high ductility and 200–800 MPa compressive strength. *ACI SP*144, 24, pp.507–18.

Sancho, J.M.; Planas, J.; Cendón, D.A.; Reyes, E.; Gálvez, J.C. (2007): An embedded crack model for finite element analysis of concrete fracture. *Engineering Fracture Mechanics*, 74, pp.75-86.

Thomas C Gasser; Gerhard A Holzapfel; (2005): Modeling 3D crack propagation in unreinforced concrete using PUFEM. *Comput Methods Appl Mech Engg.*, 194, pp.2859–2896.

Xu, S.; Reinhardt, H.W. (1999a): Determination of double-K criterion for crack propagation in quasi-brittle materials, Part I: Experimental investigation of crack propagation. *Int. J. Fracture*, 98, pp.111–149.

Xu, S.: Reinhardt, H.W. (1999b): Determination of double-K criterion for crack propagation in quasi-brittle materials, Part II: analytical evaluating and practical measuring methods for three-point bending notched beams. *Int J. Fracture*, 98, pp.151–177.

Xu, S.; Zhang, X. (2008): Determination of fracture parameters for crack propagation in concrete using an energy approach. *Eng. Fract. Mech.*, 75, pp.4292–4308.

Xu, S.; Reinhardt, H. W. (1999c): Determination of double-K criterion for crack propagation in quasi-brittle materials. part III: compact tension specimens and wedge splitting specimens, *Int. J. Fract.*, 98, pp.179–193.

Xu, S.; Reinhardt, H. W. (2000): A simplified method for determining double-K fracture parameters for three-point bending tests. *Int. J. Fract.*, 104, pp.181–209.

Zhang, J.; Stang, H. (1998): Application of stress crack width relationship in predicting the flexural behavior of fiber reinforced concrete. *Cem. Concr. Res.*, 28, pp.439–452.

Zhang, J.; Victor C, Li. (2004): Simulation of crack propagation in fiber reinforced concrete by fracture mechanics. *Cement and Concrete Research*, 34, pp.333-339.

Zhang J.; christipher K.Y. Leung; Shilang X.U. (2010): Evaluation of fracture parameters of concrete from bending test using inverse analysis approaches. *Mathematicals & Structurals,* 43, pp.857-874